Bone 74 (2015) 134–139

Contents lists available at ScienceDirect

Bone

journal homepage: www.elsevier.com/locate/bone

Original Full Length Article

Intravital bone imaging by two-photon excitation microscopy to identify osteocytic osteolysis in vivo

Hiroshige Sano [a,b], Junichi Kikuta [a,c,d], Masayuki Furuya [a,c], Naoki Kondo [b], Naoto Endo [b], Masaru Ishii [a,c,d,*]

[a] Department of Immunology and Cell Biology, Graduate School of Medicine and Frontier Biosciences, Osaka University, Osaka, Japan
[b] Department of Orthopedic Surgery, Graduate School of Medical and Dental Sciences, Niigata University, Niigata, Japan
[c] WPI-Immunology Frontier Research Center, Osaka University, Osaka, Japan
[d] JST, CREST, Tokyo, Japan

ARTICLE INFO

Article history:
Received 6 October 2014
Revised 13 January 2015
Accepted 21 January 2015
Available online 24 January 2015

Edited by Sakae Tanaka

Keywords:
Osteocytic lacunae
Two-photon microscopy
Intravital imaging
Osteocyte
Osteocytic osteolysis

ABSTRACT

Bone is a highly dynamic organ in which several cell types function cooperatively. Among these, osteocytes have recently emerged as an important regulator of bone homeostasis, although their mechanism of regulation is unclear. Here, intravital bone imaging by two-photon excitation microscopy allowed us to directly visualize 'osteocytic osteolysis', or resorption of bone in the lacuno-canalicular system. Osteocyte lacunae and the canalicular network in the cortex of murine tibiae were imaged by in vivo calcein staining, and local acidification in these structures was monitored using a topically applied pH sensor. We also demonstrated that sciatic neurectomy causes significant acidification around osteocytic lacunae and enlargement of lacuno-canalicular areas. These results provide strong evidence for osteocytic osteolysis, and demonstrate that two-photon intravital microscopy is useful for analysis of this phenomenon.

© 2015 Elsevier Inc. All rights reserved.

Introduction

Osteocytes are the most abundant cellular component of bone, comprising around 90–95% of all bone cells. These cells are 'entombed' within bone tissue, but seem to survive for extended periods, up to 25 years in humans [1]. Osteocytes are terminally differentiated osteoblasts, considered dormant until recent evidence demonstrated their critical role in endocrine regulation and bone homeostasis [2–5]. Osteocytes are connected to one another via a network of cytoplasmic projections [4,5], consisting of disk-shaped osteocytic lacunae (OL) and numerous dendritic processes (canaliculi) radiating therefrom.

Since Baud reported electron micrographic observations of osteocytes' roughly bordered lacunar walls in 1962 [6], the concept of bone resorption by osteocytes, so-called 'osteocytic osteolysis', has been proposed and reviewed [7–11], although these initial histological studies provided little definite evidence. On the contrary, OL enlargement has also been attributed to an artifact of specimen preparation [12]; isolated avian osteocytes fail to resorb bone in vitro [13]. Since similar changes in OL can also be found in younger osteocytes, enlargement could result from insufficient mineralization of the periosteocytic matrix [12,14]. In addition, the irregular, variable morphology of OL presents major challenges to examination of osteocytic osteolysis.

Nevertheless, recent circumstantial evidence supports the concept [15,16]. OL enlargement was detected by lactation [17] in the presence of sclerostin [18] or microgravity [19], suggesting active regulation of the OL space and osteolysis. However, no direct evidence has yet been presented.

Over the past few years we have established a system for visualizing the bone tissues of living animals 'intravitally' under completely intact conditions [20–25]. This novel system has unraveled mechanisms of migration and functions of bone-resorbing osteoclasts and their precursors in vivo. In this study, we exploited this new imaging technique to visualize and analyze the function of osteocytes in vivo.

Materials and methods

Intravital in vivo bone tissue imaging

Intravital microscopy of mouse tibiae was performed using protocols modified from a previous study [20,21]. Briefly, mice were anesthetized with isoflurane (2.0%, vaporized in 100% oxygen), and two-thirds of the length of the medial tibia was exposed by stripping the periosteum. Exposed cortical bone tissues were observed by two-photon excitation microscopy with a custom-made stereotactic holder. The imaging system was composed of a multiphoton microscope (SP5; Leica) driven

* Corresponding author at: 2-2 Yamada-oka, Suita, Osaka 565-0871, Japan.
E-mail address: mishii@icb.med.osaka-u.ac.jp (M. Ishii).

http://dx.doi.org/10.1016/j.bone.2015.01.013
8756-3282/© 2015 Elsevier Inc. All rights reserved.

by a laser (Mai-Tai HP Ti: Sapphire; Spectraphysics) tuned to 870 nm and an upright microscope (DM6000B; Leica) equipped with a 20× water immersion objective (HCX APO, N.A. 1.0; Leica). Fluorescent materials were detected through band pass emission filters at 430/80 nm (for second harmonic generation; SHG), at 500/50 nm (for calcein) and at 565/605 nm (for RhP-EF). Raw imaging data was processed using the Imaris software (Bitplane) with a Gaussian noise filter.

Bone labeling with calcein

Calcein (Sigma-Aldrich, 20 mg/kg, s.c.) was systemically administered the day before histological examination. Femurs were removed and frozen in chilled hexane (Wako, Osaka, Japan) on dry ice. Sections (10 μm thick) of non-decalcified femurs were subjected to bright-field and fluorescence microscopy. For intravital in vivo imaging using two-photon microscopy, calcein (20 mg/kg, s.c.) was injected 3 days before examination; injection the day before caused over-staining, preventing quantification (data not shown).

RhP-EF staining

RhP-EF (AcidiFluor™ ORANGE, Goryo Chemical (Hokkaido, Japan); 10 μM in PBS) was applied topically to the exposed bone surface for 20 min, followed by thorough washing with PBS before observation by intravital two-photon microscopy.

Image analysis

All images were captured at a 0.5-μm volume step size. The area of the largest OL from each sequential image was measured using Image J. Fluorescence intensity and length were measured using Leica TCS SP5 software. For standardization of image acquisition, OLs were selected only at depths of 15 to 25 μm beneath the bone surface. We chose OLs sufficiently labeled with calcein for analysis because we could not correctly detect the sizes of the OLs if staining deficits were present (data not shown). The areas of five randomly selected OLs were measured in each analysis, and five analyses were performed in each mouse. Fluorescent ratios were measured in three OLs per analysis. We obtained the image data exactly 20 μm below the exposed surface to detect the actual values of the fluorescent signals of RhP-EF in three randomly selected OLs per analysis.

Bone loss model with sciatic neurectomy

C57BL/6 mice at 9 weeks of age were obtained from CLEA Japan. All mice were bred and maintained under pathogen-free conditions in the animal facilities of Osaka University (Osaka, Japan). Ten-week-old female C57BL/6 mice were subjected to unilateral sciatic neurectomy (SNR) or sham surgery (day 0) under isoflurane-induced anesthesia. SNR consisted of resecting a 3- to 4-mm segment of the right sciatic nerve posterior to the hip joint [26,27]. For sham surgery, the same procedure was performed without resection.

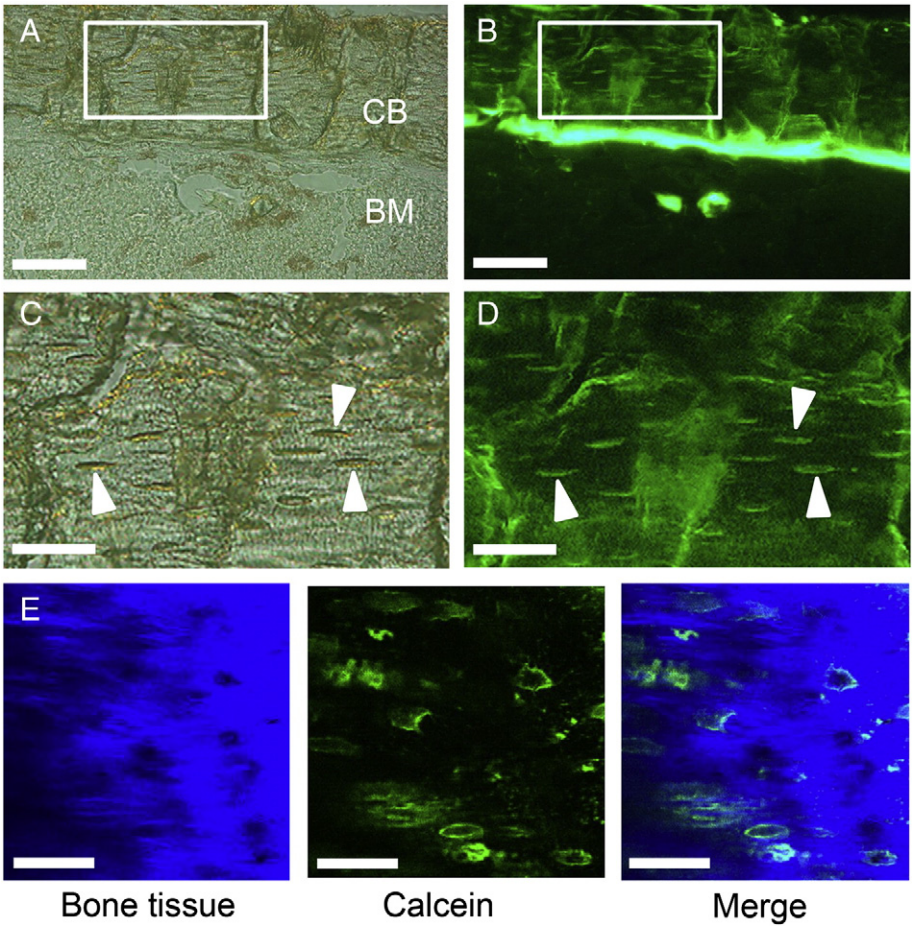

Fig. 1. Osteocytes incorporate calcein in the OL. Representative bright-field (A, C) and fluorescence microscopy (B, D) images of the middle femur 1 day following s.c. injection. (C, D) High magnification of the boxed areas in A and B, respectively. Arrowheads indicate OLs. (E) Intravital two-photon imaging of tibia cortex 3 days after calcein injection. Blue, SHG signal from collagen; green, calcein. CB: cortical bone, BM: bone marrow. Scale bars: (A, B) 100 μm; (C–E) 35 μm.

Micro-computed tomography

Trabecular bone morphometry within the metaphyseal region of the proximal tibia was quantified using micro-computed tomography (μCT) (ScanXmate-RX; Comscantechno, Kanagawa, Japan). 3D microstructural image data were reconstructed, and structural indices, such as BV/TV (%), Tb. Th. (μm), Tb. Sp. (μm) and Tb. N. (1/mm), were calculated using TRI/3D-BON software (RATOC Systems, Tokyo, Japan). Bone morphometric analysis was performed as described previously [28].

Statistical analysis

Two-tailed *t* tests were performed using the GraphPad Prism software (GraphPad, La Jolla, CA) to calculate *p* values. Data represented means ± SD. A *p* value of <0.05 was considered to indicate statistical significance.

Study approval

All animal experiments were performed according to institutional guidelines under protocols approved by the Animal Experimental Committee of Osaka University.

Results

Intravital two-photon microscopy of the osteocytic lacuno-canalicular system

To visualize the osteocytic lacuno-canalicular system in bone, we systemically administered calcein, a commonly used fluorescent dye that attaches to the bone surface (20 mg/kg, s.c.) [29]. Histological examination of femur cortical bone specimens revealed that calcein was successfully incorporated in OLs (Fig. 1A–D). Intravital two-photon imaging of live tibia cortex also detected calcein-labeled OLs (shown in green), buried in bone matrices represented by second harmonic generation (SHG) signal (blue) (Fig. 1E, Supplementary Video 1). Dots labeled with calcein were also detected around OLs, likely corresponding to osteocytic canaliculi.

Acidification in osteocytic lacunae

Osteolysis is associated with acidification of areas to be resorbed. To detect local pH around OLs, we used RhP-EF, a rhodamine-based

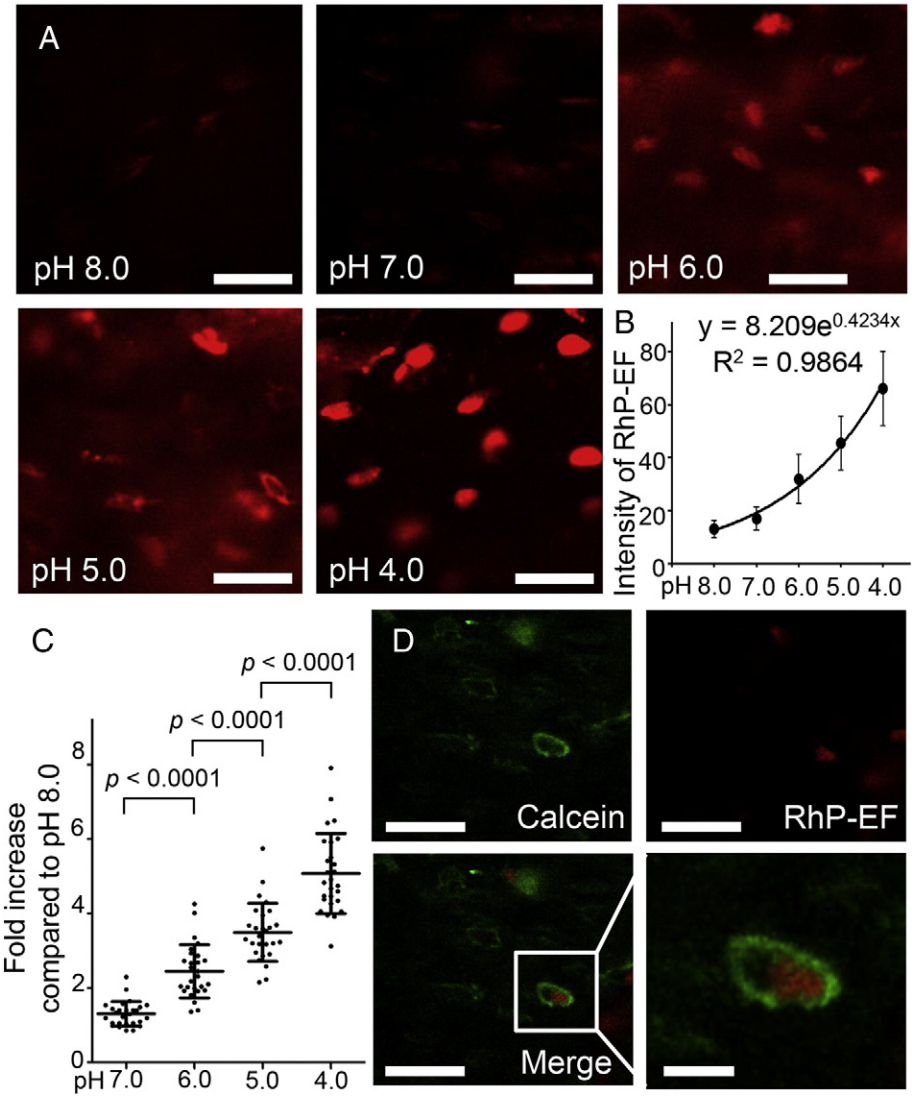

Fig. 2. RhP-EF detects acidification in OLs. (A, B) RhP-EF fluorescence following immersion of tibiae in media of various pH values for 24 h. (A) Fluorescence images (20 μm below the exposed surface). (B) Standard curve for estimating local acidification. The black dots represent the values of actual fluorescence intensity at each pH, and the line is an exponential standard curve of the data ($R^2 = 0.9864$). Error bar, mean ± SD. (C) Quantification of fluorescence intensity in OLs compared to the average intensity of pH 8.0. Three regions of interest (OLs) were analyzed in each analysis, and three analyses were performed in each experiment. Three independent experiments were performed. (D) Dual labeling of live tibial bones with calcein (administered systemically) and RhP-EF (applied topically). Scale bars: (A, D except right lower panel in D) 35 μm; (C, right lower panel) 10 μm.

fluorescent pH sensor [30,31], because rhodamine 6G applied to exposed bone surfaces penetrates deep into bone trabeculae to allow visualization of osteocytic canalicular networks (Supplementary Fig. 1). To examine the applicability of this pH probe, tibiae were resected and immersed in media of various pH values for 24 h and RhP-EF (10 μM in PBS) was applied topically (Fig. 2A). Fluorescence intensity was correlated with proton concentration (lower pH) (Fig. 2B, C), suggesting that RhP-EF is an effective indicator of pH in OLs in bone tissue.

Dual labeling of live tibiae with systemically administered calcein and topically applied RhP-EF identified a red fluorescent signal around some, but not all, OL structures visualized by calcein (Fig. 2D). This finding indicated local acidification in only some OLs.

Sciatic neurectomy reduces bone density while increasing area and reducing pH in OLs

Sciatic neurectomy (SNR) has been reported as a means of inducing severe osteoporosis [26,27]. As in previous studies, we also demonstrated significantly lower bone density in the proximal tibiae from 10 days after SNR than in sham-operated mice by μCT (Fig. 3A–C, Supplementary Fig. 2). Decreased bone density lead to osteoclastic bone resorption as well as osteocytic osteolysis. Next, we observed OL morphology and acidification by two-photon microscopy (Fig. 3D–G). Finally, we evaluated the OL area and the ratio of linear fluorescent signals of RhP-EF and calcein around the OLs (Fig. 3H). OLs were significantly enlarged following SNR (141.9 ± 40.0 vs.

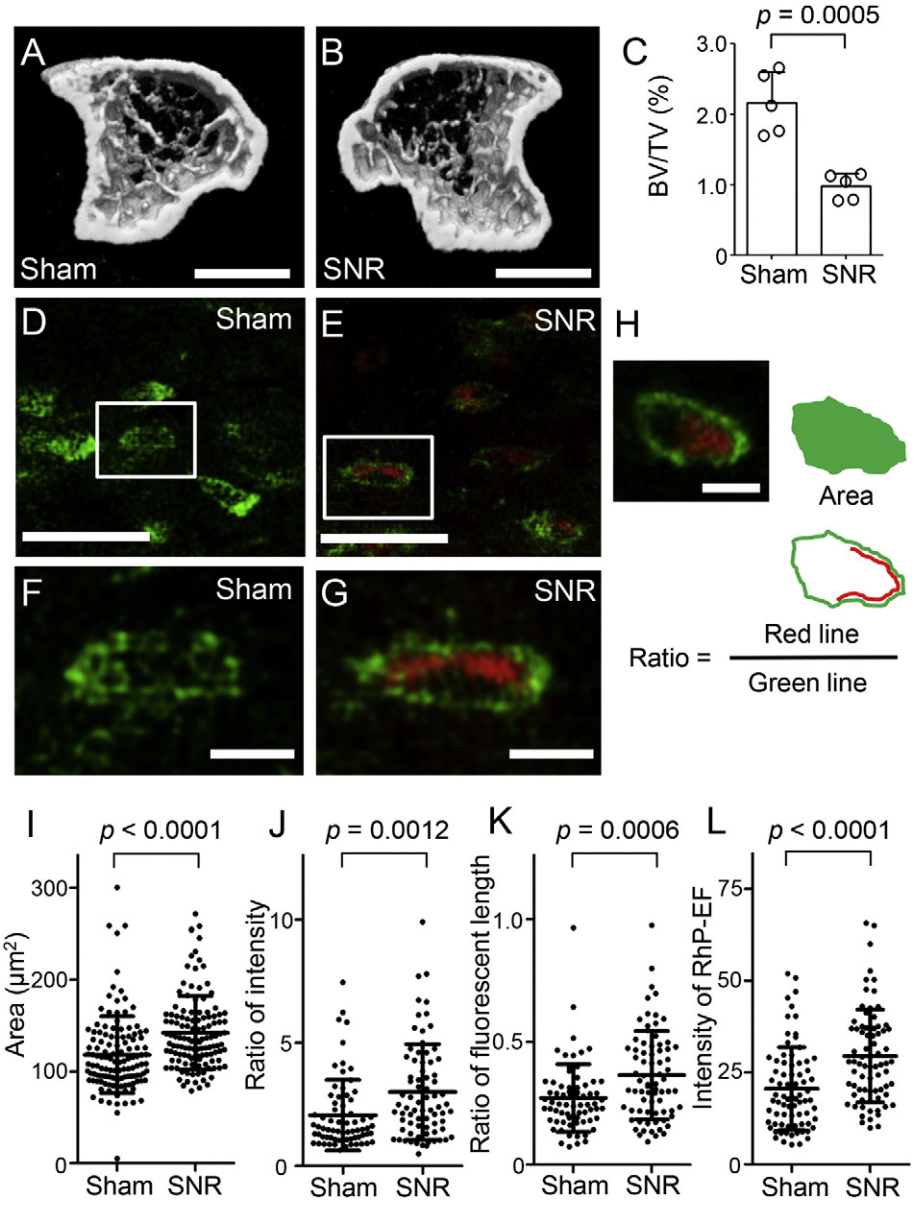

Fig. 3. SNR reduces bone density and causes OL enlargement and acidification in proximal tibiae. (A, B) Representative cross-sectional μCT images of the proximal metaphyseal region. (C) BV/TV 10 days after SNR or sham surgery (n = 5 in each group). (D–G) Dual labeling with calcein (systemically administered) and RhP-EF (topically applied) visualized by intravital two-photon microscopy. OLs were selected at 15–25 μm beneath the bone surface. (F, G) Highly magnified images of the boxed areas in D and E, respectively. (H) Schematic representation of OL analysis. Green line, OL surface labeled with calcein. Red line, acidified area (activated RhP-EF) in contact with the OL. The area surrounded by the green line and the length and mean intensity of the red and green lines were measured. Ratios of intensity and length were calculated as red:green. This image was taken from Fig. 2C. (I) OL area (n = 5 mice, 125 OLs counted in each group). (J, K) Ratio of average intensity of RhP-EF fluorescence to that of calcein (J), and the proportion of OL surfaces in contact with RhP-EF fluorescence (K). (n = 5, 75 OLs in SNR and 70 in sham). In the sham group, five OLs from two mice were excluded from the analysis because of the difficulty in distinguishing calcein and RhP-EF fluorescence. (L) Actual values of fluorescent signals of RhP-EF in contact with the OLs. Based on the standard curve shown in Fig. 2B, the absolute pH values were estimated as 6.8 (sham) and 5.9 (SNR). Scale bars: (A, B) 1 mm; (D, E) 35 μm; (F–H) 10 μm.

119.0 ± 40.5 μm^2; $p < 0.0001$) (Fig. 3I). In addition, the average red RhP-EF fluorescent intensity over all OL surfaces (calculated following the equation shown in Fig. 3H) was greater in mice with resected SNs than in sham-operated mice (3.01 ± 1.94 vs. 2.07 ± 1.43 a.u.; $p = 0.0012$) (Fig. 3J). Moreover, the ratio of the OL surface with RhP-EF fluorescence to the total OL surface (also calculated following the equation shown in Fig. 3H) was significantly enlarged following SNR (0.37 ± 0.18 vs. 0.27 ± 0.14; $p = 0.0006$), suggesting more frequent osteocytic osteolysis in OL areas (Fig. 3K). We also quantified the fluorescent intensity of RhP-EF (21.12 ± 11.57 and 30.00 ± 13.11 in sham-operated and SNR conditions, respectively; $p < 0.0001$) (Fig. 3L). Based on the standard curve shown in Fig. 2B, the pH values in the OL areas were estimated as 6.8 (sham) and 5.9 (SNR). The acidification induced by SNR (pH of approximately 5.9) would be sufficient for osteolysis because the pH values in the osteoclastic resorption pits were within the range of 4 to 6 in vivo [23,32].

Discussion

The function of osteocytes in bone metabolism has been discussed extensively, but numerous controversies remain. Among these, osteolysis is especially anecdotal, because most studies so far have employed histological analyses, providing no direct evidence. In this study, by using intravital bone imaging with fluorescent probes, we have found strong evidence for acidification in osteocytic lacunae in osteoporotic conditions such as sciatic neurectomy. Because acidification is a key step in resorbing bone matrices, it is plausible that osteolysis indeed occurs in these areas.

Several reports oppose the idea that osteocytes resorb bone. For example, Qing et al. reported that mechanical disuse caused by tail suspension induces rapid bone loss, but cortical OL area did not change [17]. This observation contradicts the present result, although we noticed that the OL areas they measured were much smaller than those in our study (29.30 ± 1.95 μm^2 in their report and 119.0 ± 40.5 μm^2 in our study). This discrepancy could be due to differences in sectioning methods; the OL is disk-shaped, and the two dimensions differ greatly in length [19]. One of the major advantages of intravital bone imaging is that it allows for visualization without sectioning, revealing the entire 3D structure of OLs and enabling the precise measurement of OL size. However, we cannot exclude the possibility that calcein labeling results in some OL shape artifacts because calcein deposition is limited on the mineralized bone surfaces [29].

Unlike osteoclasts, which are specialized for resorbing bone through acidification by proton pumps and degradation by cathepsins, how osteocytes secrete protons and how this process is regulated are unclear. Nevertheless, accumulating evidence indicates that sclerostin is involved in catabolism in the OL. Sclerostin was recently reported to induce a decrease in the intracellular and extracellular pH in human primary osteocyte-like cells as well as murine MLO-Y4 cells [18]. In addition, Moustafa et al. reported that sciatic neurectomy induces expression of sclerostin in osteocytes and reduces bone density [33]. Taken together, these findings suggest that sclerostin may play a key role in activating osteocytic osteolysis following SNR. Moreover, Blaber et al. [19] recently reported that the number of TRAP-positive osteocytes in femoral cortical bone increased in response to space flight. Qing et al. [17] revealed that the expression of osteoclast-specific genes, such as TRAP, cathepsin K, ATP6V0D2, ATP6V1G1, carbonic anhydrase 1 and 2, Nhedc2, and MMP13, is higher in osteocytes during lactation. Thus, these genes may be other potential contributors to osteocytic osteolysis. Despite progress in understanding of osteocytic osteolysis, several key questions remain to be addressed, such as the identity of factors that regulate acidification, mechanisms of acidification and the local physiological implications of osteolysis. The method presented in this study is a novel tool for studying bone biology and will be useful for clarifying these questions in future studies.

Supplementary data to this article can be found online at http://dx.doi.org/10.1016/j.bone.2015.01.013.

Disclosures

All authors declare that they have no conflicts of interest.

Acknowledgments

We thank Drs. K. Kikuchi, T. Kowada and H. Maeda (Osaka University Graduate School of Engineering) and H. E. Takahashi, N. Yamamoto and T. Shimakura (Niigata Bone Science Institute) for helpful discussions. This work was funded by Grants-in-Aid for Scientific Research on Innovative Areas (22113007), by Grant-in-Aid for Scientific Research (A) (25253070) from the Ministry of Education, Science, Sports and Culture of Japan, by grants from the International Human Frontier Science Program (RGY0077/2011); and by grants from the Takeda Science Foundation and Uehara Memorial Foundation.

References

[1] Franz-Odendaal TA, Hall BK, Witten PE. Buried alive: how osteoblasts become osteocytes. Dev Dyn 2006;235:176–90.
[2] Nakashima T, Hayashi M, Fukunaga T, Kurata K, Oh-Hora M, Feng JQ, et al. Evidence for osteocyte regulation of bone homeostasis through RANKL expression. Nat Med 2011;17:1231–4.
[3] Xiong J, Onal M, Jilka RL, Weinstein RS, Manolagas SC, O'Brien CA. Matrix-embedded cells control osteoclast formation. Nat Med 2011;17:1235–41.
[4] Atkins GJ, Findlay DM. Osteocyte regulation of bone mineral: a little give and take. Osteoporos Int 2012;23:2067–79.
[5] Bonewald LF. The amazing osteocyte. J Bone Miner Res 2011;26:229–38.
[6] Baud CA. Morphology and inframicroscopic structure of osteocytes. Acta Anat (Basel) 1962;51:209–25.
[7] Qing H, Bonewald LF. Osteocyte remodeling of the perilacunar and pericanalicular matrix. Int J Oral Sci 2009;1:59–65.
[8] Teti A, Zallone A. Do osteocytes contribute to bone mineral homeostasis? Osteocytic osteolysis revisited. Bone 2009;44:11–6.
[9] Wysolmerski JJ. Osteocytes remove and replace perilacunar mineral during reproductive cycles. Bone 2013;54:230–6.
[10] Wysolmerski JJ. Osteocytic osteolysis: time for a second look? Bonekey Rep 2012;1:229.
[11] Arnett TR. Osteocytes: regulating the mineral reserves? J Bone Miner Res 2013;28:2433–5.
[12] Parfitt AM. The cellular basis of bone turnover and bone loss: a rebuttal of the osteocytic resorption—bone flow theory. Clin Orthop Relat Res 1977;236–47.
[13] van der Plas A, Aarden EM, Feijen JH, de Boer AH, Wiltink A, Alblas MJ, et al. Characteristics and properties of osteocytes in culture. J Bone Miner Res 1994;9:1697–704.
[14] Boyde A, Jones SJ. Estimation of the size of resorption lacunae in mammalian calcified tissues using SEM stereophotogrammetry. Scan Electron Microsc 1979;393–402.
[15] Tazawa K, Hoshi K, Kawamoto S, Tanaka M, Ejiri S, Ozawa H. Osteocytic osteolysis observed in rats to which parathyroid hormone was continuously administered. J Bone Miner Metab 2004;22:524–9.
[16] Lane NE, Yao W, Balooch M, Nalla RK, Balooch G, Habelitz S, et al. Glucocorticoid-treated mice have localized changes in trabecular bone material properties and osteocyte lacunar size that are not observed in placebo-treated or estrogen-deficient mice. J Bone Miner Res 2006;21:466–76.
[17] Qing H, Ardeshirpour L, Pajevic PD, Dusevich V, Jahn K, Kato S, et al. Demonstration of osteocytic perilacunar/canalicular remodeling in mice during lactation. J Bone Miner Res 2012;27:1018–29.
[18] Kogawa M, Wijenayaka AR, Ormsby RT, Thomas GP, Anderson PH, Bonewald LF, et al. Sclerostin regulates release of bone mineral by osteocytes by induction of carbonic anhydrase 2. J Bone Miner Res 2013;28:2436–48.
[19] Blaber EA, Dvorochkin N, Lee C, Alwood JS, Yousuf R, Pianetta P, et al. Microgravity induces pelvic bone loss through osteoclastic activity, osteocytic osteolysis, and osteoblastic cell cycle inhibition by CDKN1a/p21. PLoS One 2013;8:e61372.
[20] Ishii M, Egen JG, Klauschen F, Meier-Schellersheim M, Saeki Y, Vacher J, et al. Sphingosine-1-phosphate mobilizes osteoclast precursors and regulates bone homeostasis. Nature 2009;458:524–8.
[21] Ishii M, Kikuta J, Shimazu Y, Meier-Schellersheim M, Germain RN. Chemorepulsion by blood S1P regulates osteoclast precursor mobilization and bone remodeling in vivo. J Exp Med 2010;207:2793–8.
[22] Ishii M, Fujimori S, Kaneko T, Kikuta J. Dynamic live imaging of bone: opening a new era with 'bone histodynametry'. J Bone Miner Metab 2013;31:507–11.
[23] Kikuta J, Wada Y, Kowada T, Wang Z, Sun-Wada GH, Nishiyama I, et al. Dynamic visualization of RANKL and Th17-mediated osteoclast function. J Clin Invest 2013;123:866–73.
[24] Kikuta J, Kawamura S, Okiji F, Shirazaki M, Sakai S, Saito H, et al. Sphingosine-1-phosphate-mediated osteoclast precursor monocyte migration is a critical point of

control in antibone-resorptive action of active vitamin D. Proc Natl Acad Sci U S A 2013;110:7009–13.
[25] Kotani M, Kikuta J, Klauschen F, Chino T, Kobayashi Y, Yasuda H, et al. Systemic circulation and bone recruitment of osteoclast precursors tracked by using fluorescent imaging techniques. J Immunol 2013;190:605–12.
[26] Landry M, Fleisch H. The Influence of immobilisation on bone formation as evaluated by osseous incorporation of tetracyclines. J Bone Joint Surg Br 1964;46:764–71.
[27] Klein L, Kanefield DG, Heiple KG. Effect of disuse osteoporosis on bone composition: the fate of bone matrix. Calcif Tissue Res 1968;2:20–9.
[28] Parfitt AM, Drezner MK, Glorieux FH, Kanis JA, Malluche H, Meunier PJ, et al. Bone histomorphometry: standardization of nomenclature, symbols, and units. Report of the ASBMR Histomorphometry Nomenclature Committee. J Bone Miner Res 1987;2:595–610.
[29] Turner RT. Cancellous bone turnover in growing rats: time-dependent changes in association between calcein label and osteoblasts. J Bone Miner Res 1994;9:1419–24.
[30] Urano Y, Asanuma D, Hama Y, Koyama Y, Barrett T, Kamiya M, et al. Selective molecular imaging of viable cancer cells with pH-activatable fluorescence probes. Nat Med 2009;15:104–9.
[31] Urano Y, Kamiya M, Kanda K, Ueno T, Hirose K, Nagano T. Evolution of fluorescein as a platform for finely tunable fluorescence probes. J Am Chem Soc 2005;127:4888–94.
[32] Kowada T, Kikuta J, Kubo A, Ishii M, Maeda H, Mizukami S, et al. In vivo fluorescence imaging of bone-resorbing osteoclasts. J Am Chem Soc 2011;133:17772–6.
[33] Moustafa A, Sugiyama T, Prasad J, Zaman G, Gross TS, Lanyon LE, et al. Mechanical loading-related changes in osteocyte sclerostin expression in mice are more closely associated with the subsequent osteogenic response than the peak strains engendered. Osteoporos Int 2012;23:1225–34.